NASA TECHNICAL NOTE

NASA TN D-2446

c 1

NASA TN D-2446

TECH LIBRARY KAFB, NM

0079568

EXPERIMENTAL TECHNIQUE FOR MEASURING TOTAL AERODYNAMIC HEATING RATES TO BODIES OF ARBITRARY SHAPE WITH RESULTS FOR MACH 7

by L. Roane Hunt and R. R. Howell

Langley Research Center
Langley Station, Hampton, Va.

NATIONAL AERONAUTICS AND SPACE ADMINISTRATION • WASHINGTON, D. C. • SEPTEMBER 1964

TECH LIBRARY KAFB, NM

0079568

EXPERIMENTAL TECHNIQUE FOR MEASURING TOTAL AERODYNAMIC HEATING RATES TO BODIES OF ARBITRARY SHAPE WITH RESULTS FOR MACH 7

By L. Roane Hunt and R. R. Howell

Langley Research Center
Langley Station, Hampton, Va.

NATIONAL AERONAUTICS AND SPACE ADMINISTRATION

For sale by the Office of Technical Services, Department of Commerce,
Washington, D.C. 20230 -- Price $1.00

EXPERIMENTAL TECHNIQUE FOR MEASURING TOTAL AERODYNAMIC HEATING RATES TO BODIES OF ARBITRARY SHAPE WITH RESULTS FOR MACH 7

By L. Roane Hunt and R. R. Howell
Langley Research Center

SUMMARY

A liquid-metal expansion technique for measuring the total heating rate to bodies of arbitrary shape is described. The calibration and test procedures required to afford useful data from the technique are delineated. In addition, the results obtained from three types of apparatus are presented to indicate the accuracy and reliability of the technique.

In general, the experimental results for a Mach number of 7 show that total aerodynamic heating rates to arbitrarily shaped bodies can be accurately defined with the technique. Use of the technique should permit accurate experimental studies of total aerodynamic heating. As a result of the simplicity of the technique, reliable total-heating-rate data should also be obtained easily.

INTRODUCTION

With the advent of hypersonic reentry vehicles whose geometries are complex, the need for adequate means for obtaining information concerning heat transfer to such vehicles becomes increasingly important. It is impossible to design an efficient thermal protection system for these vehicles without a complete quantitative picture of the heating to be experienced by the vehicle. Heat-transfer information is not only required for areas of the vehicles which experience high local heating rates, but the total heating rate to the entire vehicle is also important inasmuch as this is the quantity of heat that must be either absorbed or blocked by a thermal protection system.

Since the vehicle shape (hence the flow over it) is complex, existing theories cannot accurately predict the distribution of local heating rates, or the total heating rate. Hence, experimentation must be employed to provide this information. Previously used experimental techniques for the determination of total heating rates, such as the measurement of the temperature rise of water as it passes into and out of a body or the use of calorimeters to measure local heating rates, have disadvantages and limitations in their application to complex aerodynamic shapes.

Although methods of measuring total aerodynamic heating rates to complex shapes are presently being explored (see, for example, ref. 1), the accuracy and limitations of the approaches are not considered adequate for the solution of all total-heat-transfer-rate problems.

The present paper presents one method of measuring total heating rates directly. The technique, which involves the measuring of the rate of expansion of a volume of liquid metal, has been developed and experimental data are presented to indicate the accuracy of the system under various modes of heat input. Some aerodynamic tests to determine the total heating rates were performed in the 7-inch Mach 7 pilot tunnel at the Langley Research Center. The experimental results from these tests are presented and compared, where possible, with other experimental results and with theory.

SYMBOLS

The units used for the physical quantities defined in this section are given in both U.S. customary units and in the International System of Units (SI). (See ref. 2.) The conversion factors required for units used in the present study are presented in appendix A.

A	area, ft^2 (m^2)
c_p	specific heat at constant pressure, Btu/lb-$^{\circ}$R (J/g-$^{\circ}$K)
k	thermal conductivity, Btu/sec-ft-$^{\circ}$R (W/m-$^{\circ}$K)
l	cylinder length, in. (m)
m	mass, lb (g)
p	pressure, psia $\left(MN/m^2\right)$
$\dot{q}$	local heating rate, Btu/ft^2-sec $\left(MW/m^2\right)$
$\dot{Q}$	total heating rate, Btu/sec (W)
r	model nose radius, in. (m)
s	distance along meridian profile of body, measured from model stagnation point, in. (m)
S	model surface area excluding base portion, ft^2 (m^2)
t	time, sec
T	temperature, $^{\circ}$R ($^{\circ}$K)
$\overline{T}$	mean temperature of liquid metal, $^{\circ}$R ($^{\circ}$K)

v	specific volume, in.^{3}/lb $\left(cm^3/g\right)$
V	volume, in.^{3} $\left(m^3\right)$
x	longitudinal distance between model and lamps, in. (m)
α	angle of attack, deg
θ	angle between inward body surface normal and stream direction, deg
μ	absolute viscosity, lb/ft-sec $\left(Ns/m^2\right)$
ρ	mass density, lb/ft^3 $\left(g/m^3\right)$
σ	surface tension, lb/ft (N/m)
τ	plate thickness, in. (m)
ψ	angle of yaw, deg

Subscripts:

ex	exposed
s	stagnation point
t	total condition
ws	wall value at stagnation point

DISCUSSION OF THE TECHNIQUE

The technique requires monitoring the volumetric expansion of a known mass of liquid metal which is subjected to external heating. The liquid metal is chosen such that the volumetric expansion with change in mean temperature $\left(\frac{\partial V}{\partial \overline{T}}\right)$ is constant over the range of temperature to be experienced by the metal. Hence, the rate of change of the mean temperature of the metal may be defined as $\frac{\partial \overline{T}}{\partial t} = \frac{\partial V}{\partial t}\frac{\partial \overline{T}}{\partial V}$. The total heating rate to the metal is then defined by the product of the mass, its specific heat, and the rate of change of its mean temperature with time (which is defined by volume change rate) as follows:

$$\dot{Q} = \int_S \dot{q}\, dS = mc_p \frac{\partial \overline{T}}{\partial V}\frac{\partial V}{\partial t} \tag{1}$$

In this equation, the metal mass m and its specific heat c_p are known. The net change in liquid metal volume with change in mean temperature $\left(\frac{\partial V}{\partial \bar{T}}\right)$ is determined by calibration of the specific model to be tested, whereas the rate of change of net volume with time $\left(\frac{\partial V}{\partial t}\right)$ is measured during the test.

The necessary elements of the technique are the model shell, the liquid-metal medium, and a method by which the volumetric expansion of the liquid metal may be measured. The models used by this technique must be thin-wall metal shells that can have any shape within the limits of fabrication. The shell material must have a relatively low coefficient of thermal expansion and a high thermal conductivity. The shell wall thickness has to be a compromise based on consideration of both heat transfer and structural requirements. The thickness is desired to be a minimum to obtain high sensitivity and negligible heat conduction along the wall. The limiting factor in minimizing the wall thickness is the structural requirements to prevent significant surface deformation due to internal pressure and local thermal expansion of the shell. Other requirements would depend on the method of fabrication.

The liquid-metal medium must have a melting point well below ambient temperature and a boiling point high enough to permit the temperature rise due to heating of the liquid during tests. Also, the volumetric expansion of the liquid with temperature rise should be linear for the range of temperature to be experienced by the metal. The liquid metal used should have a relatively high thermal conductivity and heat capacity. Relatively low values of surface tension and absolute viscosity were found to be desirable in the task of filling models completely with the liquid metal. In addition, problems in handling the liquid metal must be considered.

The methods by which the liquid-metal expansion rates can be measured are numerous. The basic requirements for the system are (1) that its response be instantaneous and direct, (2) that its repeatability be good, and (3) that it be capable of functioning in a high-energy-level stream without incurring error due to extraneous thermal inputs or forces.

MODEL ASSEMBLY

Model Shell

The five model shells that were used in the experiments (figs. 1 and 2) consisted of a flat-faced cylinder (model A), three hemispherical-faced cylinders (models B, C, and D), and a delta wing-body combination (model E). The flat-faced cylinder was machined from monel. The three hemisphere-cylinder models were electroformed in nickel on aluminum mandrels; after the models were externally machined to exact dimensions, the mandrels were removed by an etching process. The delta wing-body model was centrifically cast in 302 stainless steel in a hot ceramic mold. The base and support stub were then welded in place. No machining was done to this model surface. In all

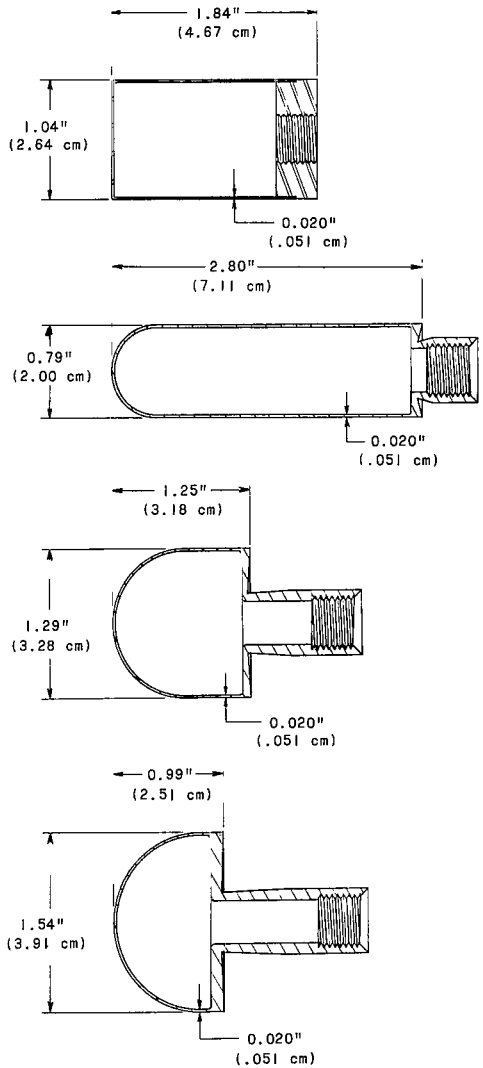

(a) Bodies of revolution.

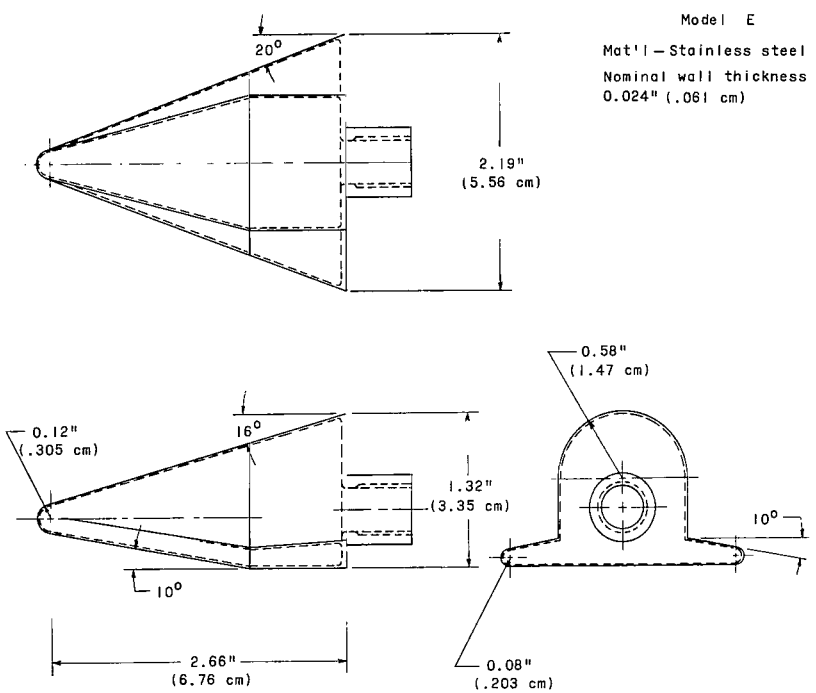

(b) Delta wing-body model.

Figure 1.- Pertinent details of models used in total-heating-rate tests.

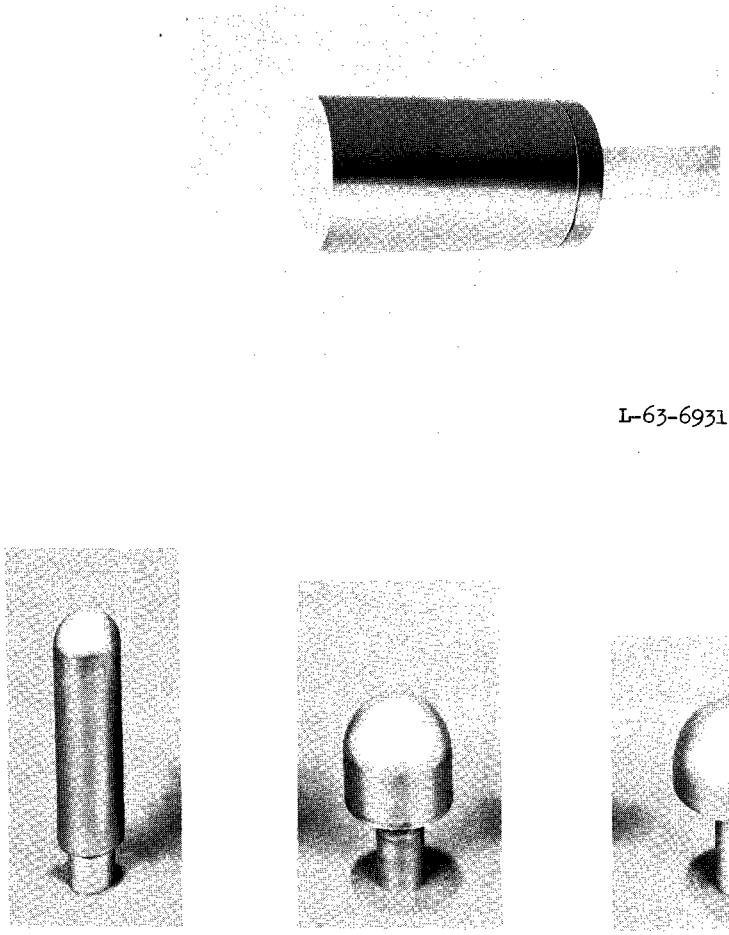

L-63-6931

L-63-3328

(a) Bodies of revolution.

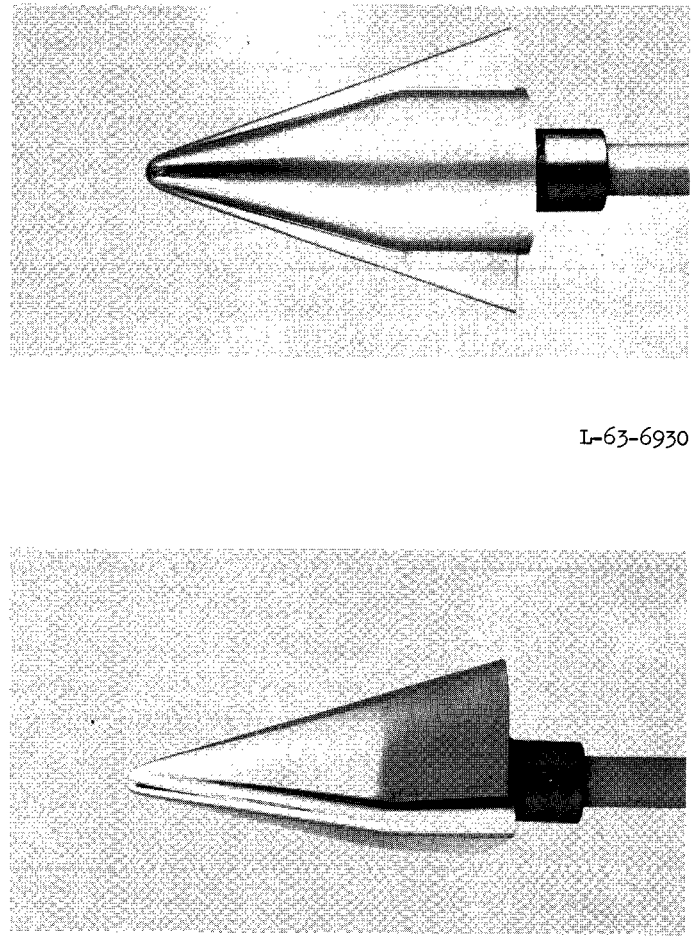

L-63-6930

L-63-6929

(b) Delta wing-body model.

Figure 2.- Photographs of models.

cases the model wall thickness was approximately 0.020 inch (0.051 cm) and the external surface was polished to about 25 microinches (0.64 μm) root mean square. Inasmuch as all the models were supported from the base, the model surface thickness at the base had to be relatively thick and was therefore not considered as part of the heat-sensing area. For aerodynamic heating in hypersonic flow, the base of the model would be located in the wake region and would, for the average configuration, contribute very little to the total heating rate.

Liquid-Metal Medium

Two liquid metals which meet the desired requirements are mercury (Hg) and a sodium-potassium alloy with a 44 percent potassium content (designated NaK). The pertinent physical properties of the two metals are presented as figure 3. The plots were made with data from references 3 and 4. Figure 3(a) is a plot of specific volume against temperature. The specific volume of both liquids varies linearly with temperature. The NaK, however, has a higher boiling point, a greater expansion for a given temperature rise, and a higher specific volume. Also, the NaK has a higher thermal conductivity (fig. 3(b)) and a much higher specific heat (fig. 3(c)). Mercury has a much higher absolute viscosity and surface tension (figs. 3(d) and 3(e)). Therefore, from the comparison given, the NaK appears to be the better liquid metal to be used with the present technique. However, liquid NaK will oxidize rapidly when exposed to water or air at elevated temperatures. Because of the added difficulties in handling of the NaK safely, mercury was used in the present exploratory investigation.

Method of Measuring Volumetric Expansion

Three general methods of measuring the expansion of the liquid metal were considered. These methods are illustrated in figure 4. The inside of the support adapter attached to the model was fabricated to form a right circular cylinder through which the liquid metal was allowed to expand. In each method, a piston was in contact with the liquid metal and moved longitudinally through the cylinder as the liquid medium expanded. The rate of the piston displacement defined the volumetric expansion rate of the liquid mass and, hence, is a direct function of the rate of total heat input to all model surfaces exposed to heating.

The first method (fig. 4(a)) detects the distance the piston travels by measuring the pressure increase of the entrapped air behind the piston. The entrapped air experienced nearly isothermal compression because the heat developed during compression was small and was rapidly conducted into the cylinder walls. For the small pressure increase of the entrapped air, the relation between pressure and volume was effectively linear. Therefore, the pressure of the entrapped air was directly proportional to the mean temperature of the mercury. This method was used in the initial localized heating tests but was found to be limited in application because of the effect of external heating on the enclosed air volume in the sting support during aerodynamic tests.

In the methods illustrated by figures 4(b) and 4(c), the piston travel is measured directly. In figure 4(b) the cantilever beam, which is instrumented

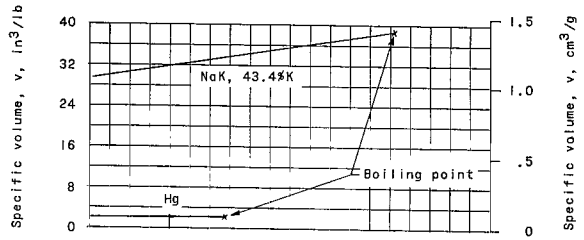

(a) Specific volume.

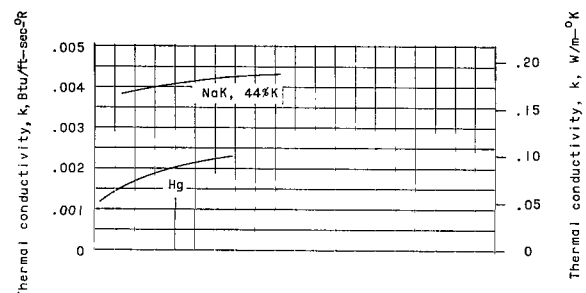

(b) Thermal conductivity.

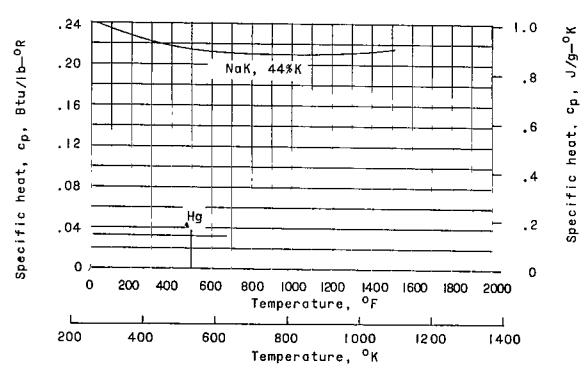

(c) Specific heat.

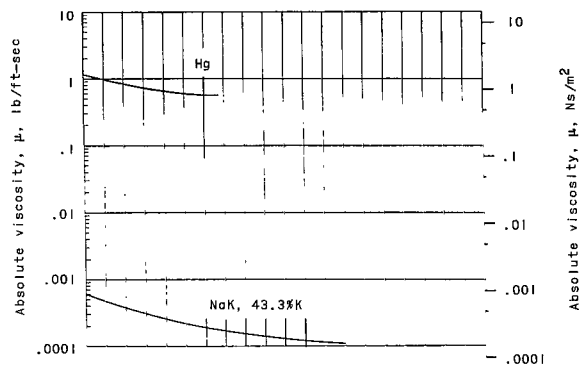

(d) Absolute viscosity.

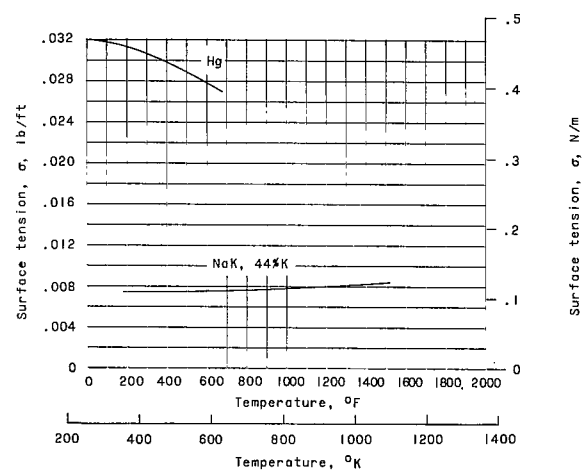

(e) Specific tension.

Figure 3.- Physical properties of two liquid metals, mercury (Hg) and sodium-potassium alloy (NaK).

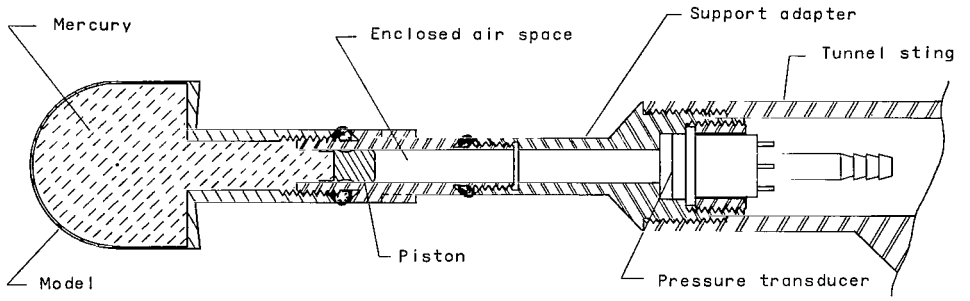

(a) Pressure transducer.

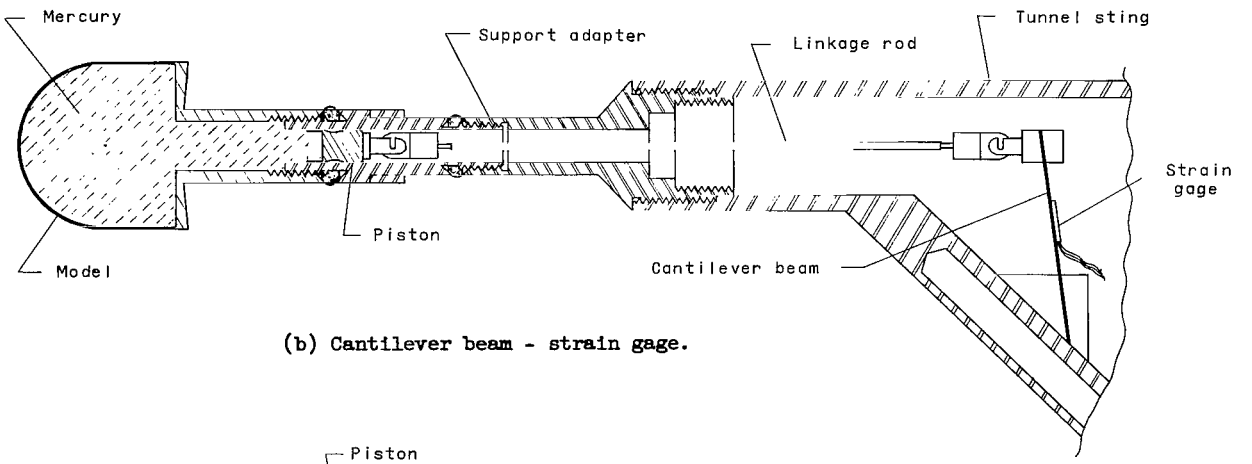

(b) Cantilever beam - strain gage.

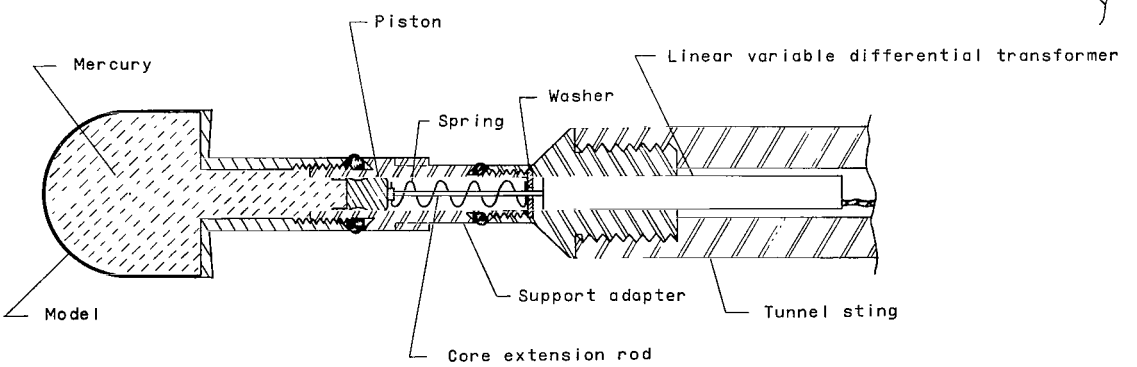

(c) Linear variable differential transformer.

Figure 4.- The various methods of measuring volumetric expansion considered during the present investigation.

by a wire strain gage, is linked directly to the piston. In figure 4(c) an inductance core is attached directly to the piston and extends through the linear variable differential transformer. Both of these methods were capable of performing the required function. However, the latter method was used in the present experimental aerodynamic testing because of its relative simplicity.

The restraining force produced by the spring on the piston (fig. 4(c)) caused the model internal pressure to increase with piston travel. A measurement of surface deflection with variations of internal pressure was made to determine the magnitude of the shape changes associated with the spring compression for model E. It was found that the deflection at the midpoint of the flat areas of the lower wing surface was about 0.004 inch (0.10 mm) at an internal pressure corresponding to the maximum spring compression. The shape changes for the hemisphere-cylinder models should have been considerably less than those for the wing-body model. Inasmuch as the deflection measured for the wing-body model was small, no consideration was given to the effect of shape change due to spring compression for the models tested.

A teflon piston was found to be the most desirable to indicate the liquid-metal expansion. Two advantages of the teflon piston are as follows: (1) The teflon to steel surface has a lower friction coefficient than other piston designs explored and (2) the teflon piston presented no crevices which tend to trap air when filling and sealing mercury within the model. The 1/4-inch-diameter (0.64-cm) teflon piston was designed to make a seal against the cylinder walls when acted upon by the pressure of the expanding mercury.

APPARATUS AND TEST PROCEDURES

In the calibration of the model assemblies and verification of the technique, three types of heating apparatus were used. A description of the apparatus and the test procedures followed is presented in the following sections.

Static Calibration

The model assemblies were statically calibrated to obtain the actual relation between the liquid-metal temperature and the piston displacement resulting from the liquid-metal expansion. The schematic illustration in figure 5 shows the calibration setup. The model assembly containing the liquid metal was suspended vertically in an oil bath. The piston, which was in contact with the liquid metal, was free to move through the cylinder. Various measuring devices such as the micrometer dial indicator shown were used to measure the piston travel. Heat to the oil bath was supplied by two variac-controlled electrical-resistance heaters. The oil-bath container was insulated to minimize heat losses. An electric mixer was used to circulate the oil and maintain even temperature in the bath. During the calibration, the temperature of the bath was increased in steps. At each step, temperature equilibrium between the oil bath and the liquid metal in the model was obtained as indicated by zero piston displacement rate. The temperature of the bath and the piston travel were then

recorded. From this calibration, a correlation was made between liquid-metal mean-temperature rise and actual piston travel (or net volumetric expansion).

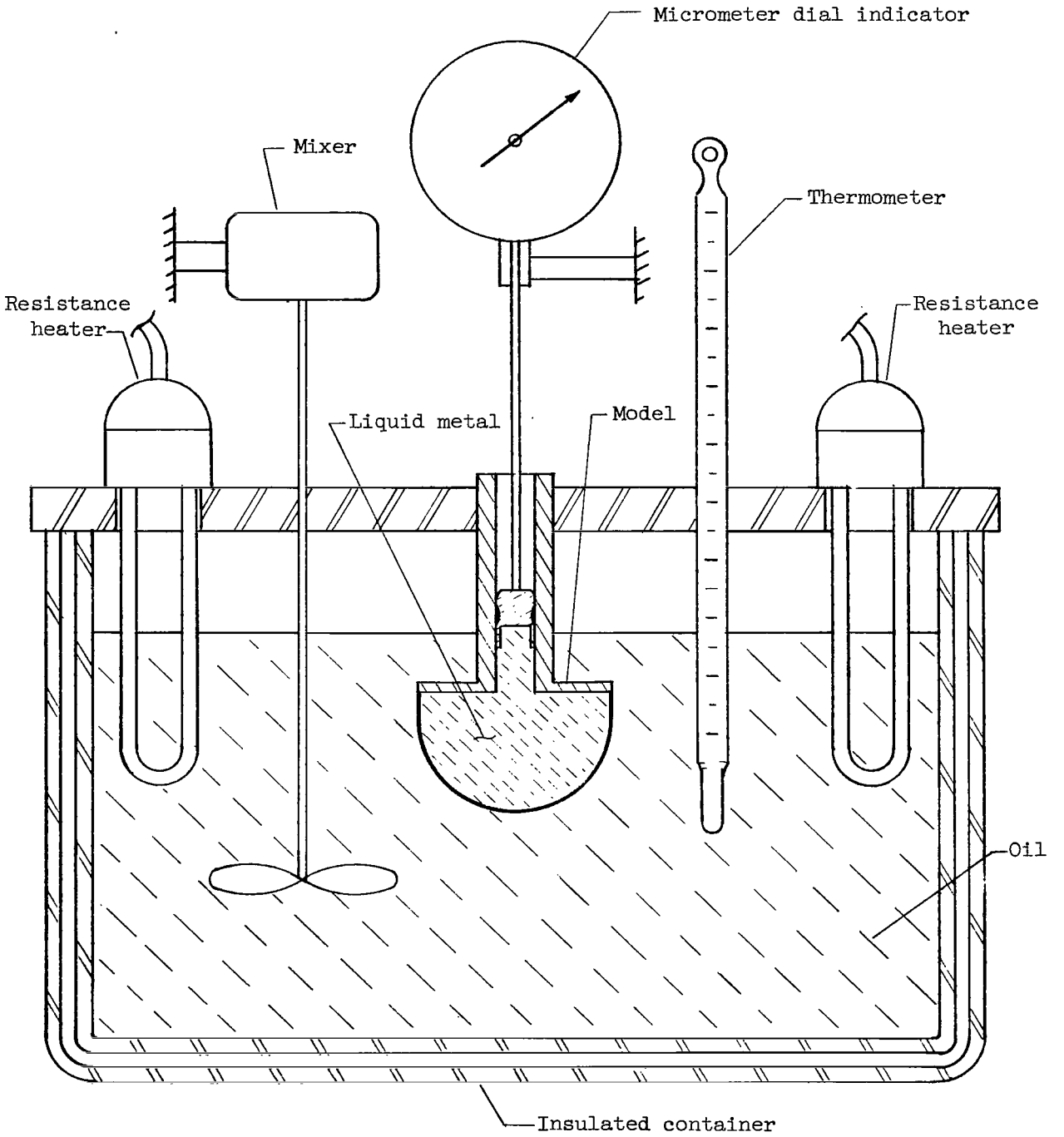

Figure 5.- Sketch showing apparatus as used for static calibration of total-heating models.

Localized Heating Tests

Two radiant-heating facilities were used in the localized heating phase of the technique evaluation. The first facility was a double bank of quartz lamps, shown schematically in figure 6. The model was mounted on a rack that could be moved along a track normal to the bank of lamps. A 6-inch × 6-inch × 1/16-inch (15.2-cm × 15.2-cm × 0.16-cm) stainless-steel plate was attached to the forward end of the rack. The face of the model was set through a hole flush with the front surface of the plate and parallel to the bank of heating lamps. Insulation was placed between the model and the plate to eliminate heat conduction or radiation to the model from the plate. The heating rate experienced by the plate was determined from the output of four chromel-alumel thermocouples which were attached to the back surface of the thin plate as indicated in figure 6. The identical heating rate was also experienced by the front face of the model; therefore, the heating rate as determined by the thermocouples was used as the reference heating rate for each test run. The heating-rate range afforded by this facility was 0 to 90 Btu/ft^2-sec (0 to 1.02 MW/m^2).

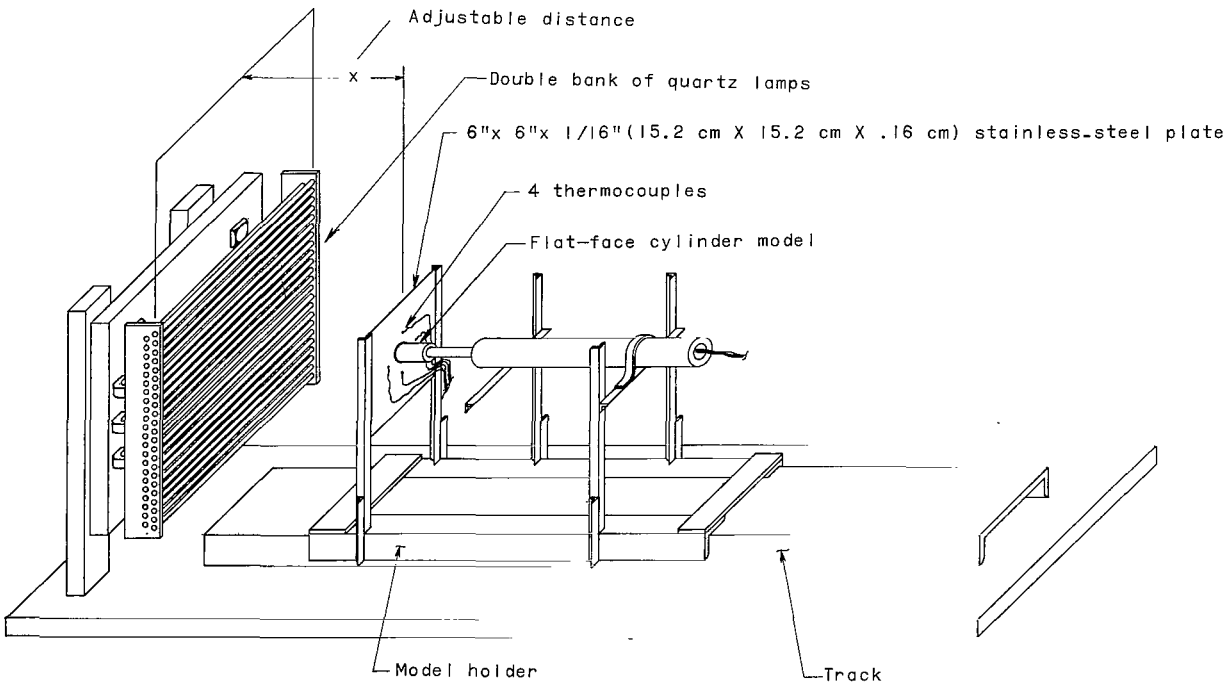

Figure 6.- Sketch showing arrangement of apparatus used in the radiant-heating tests of the flat-face cylinder model (model A).

The second radiant-heating facility used was a small arc-image furnace. The heat source for this facility was a 24-inch (61-cm) searchlight arc. The model was located near the focal point of the reflector, where maximum arc-image heating capability was concentrated. No attempt was made to vary the heating rate to the model in this facility. A copper button calorimeter was used in these tests to determine the reference heating rate. The calorimeter

temperature was indicated by the output of an attached thermocouple. The general level of the heating rate produced by this facility was approximately 185 Btu/ft^2-sec (2.1 MW/m^2).

The model used for the localized heating tests was the flat-face cylinder (model A). (See fig. 1(a).) For the testing done with the quartz lamps, the entire flat face of model A was exposed to the radiant heating. The heating rate experienced by the model was varied by adjusting the distance between the model and the bank of lamps. The variation of the heating rate with model position as afforded by temperature-time measurement is shown in figure 7. For each model position, the heating rate to the model face was also recorded by the liquid-expansion model.

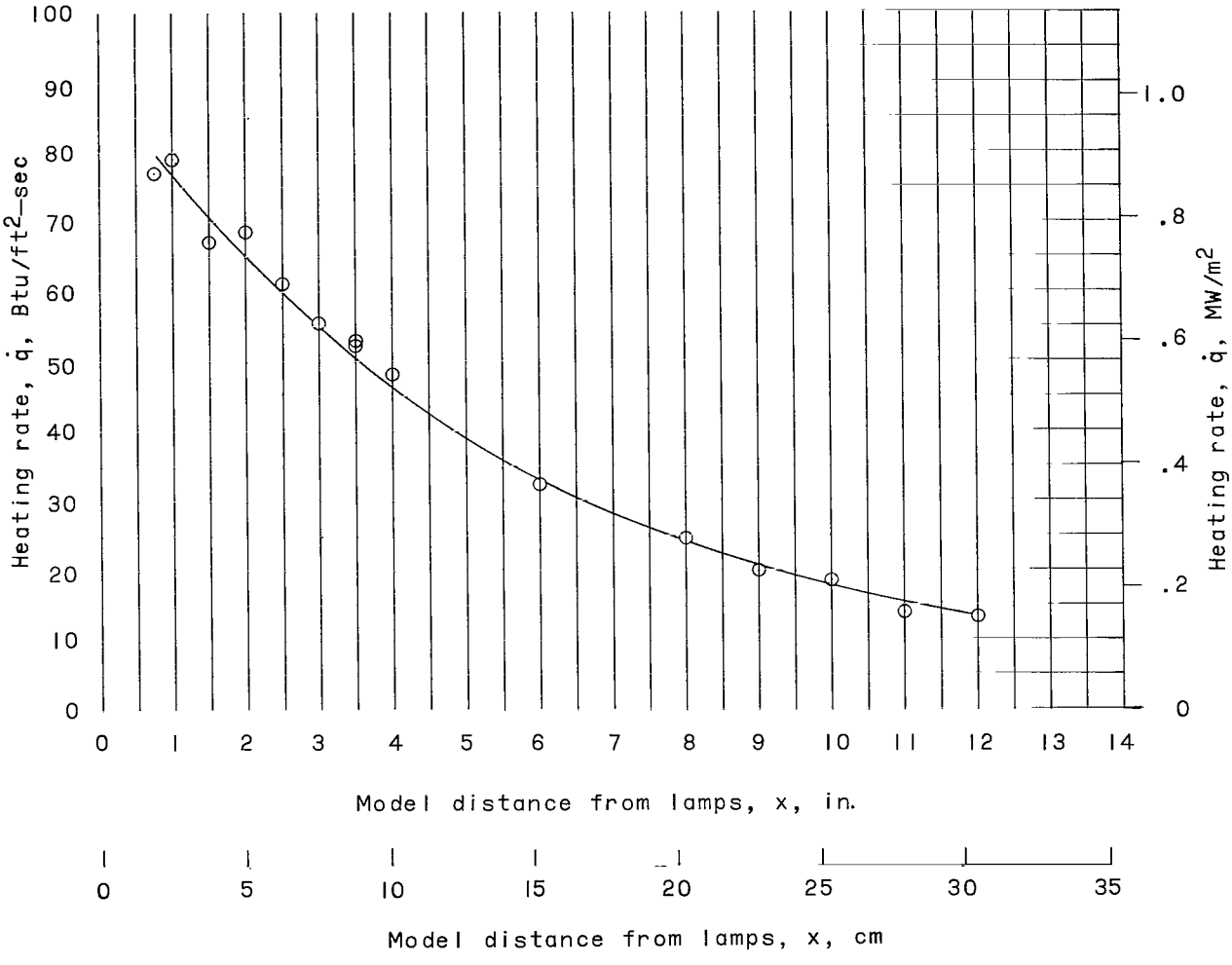

Figure 7.- Variation of surface heating rate with model position as afforded by the quartz-lamp radiant heater.

The reference heating rate indicated for the arc-image furnace is an average of three heating rates as afforded by the button calorimeter (table I). Two tests were made with the liquid-metal expansion model and the results were also averaged. For these tests, an area of the flat face of the model of only 1/4 inch (0.64 cm) in diameter was exposed to the furnace heating. From the five tests made with the furnace, a comparison was obtained between the average heating rate results afforded by the expansion model and those afforded by the calorimeter.

For each test condition the mercury expansion was recorded in terms of the pressure increase of the entrapped air within the cylindrical adapter (fig. 4(a)). The pressure transducer used was a diaphragm-type strain gage for a pressure range of ±5 psi (±35 kN/m^2). The outputs of all thermocouples, calorimeters, and transducers were recorded on an oscillograph.

Aerodynamic Heating Tests

The facility used for the aerodynamic heating tests was the 7-inch Mach 7 pilot tunnel at the Langley Research Center. This facility is a hypersonic blowdown tunnel with a high-energy level obtained by burning a mixture of methane and air under high pressure. The resulting combustion products are expanded through a nozzle and are used as the test medium. A drawing of a portion of this tunnel is shown in figure 8. Air is introduced at pressures up to 2300 psia (15.8 MN/m^2), then mixed with methane and burned in the combustion chamber. The combustion products are then expanded through the axisymmetric nozzle and pass through the free-jet test section. The flow enters the straight-tube diffuser and is pumped to the atmosphere by means of the single-stage air ejector (not shown in the drawing).

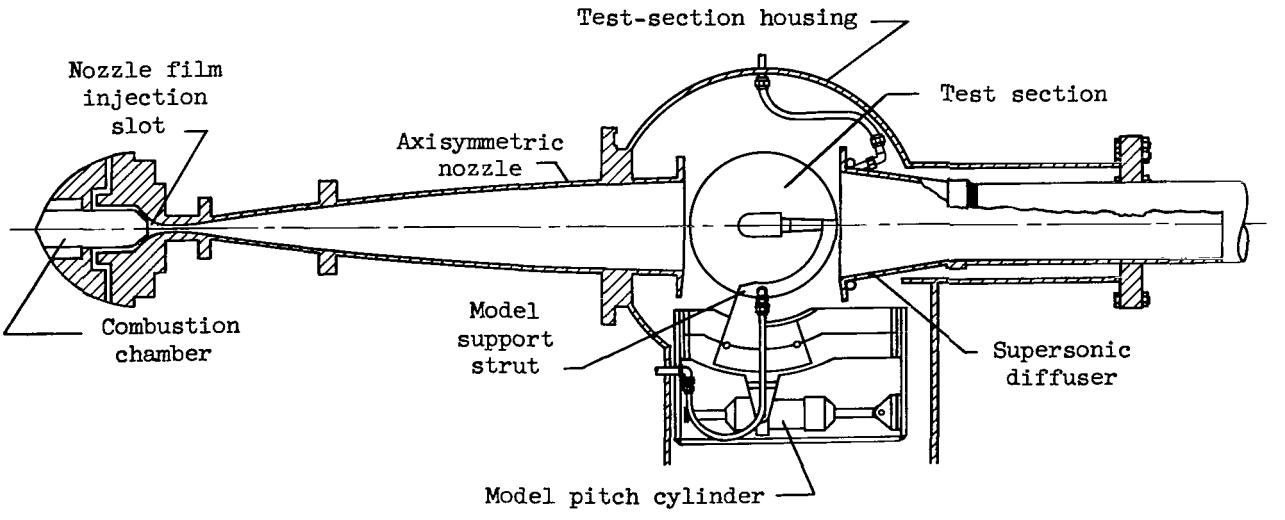

Figure 8.- Nozzle and test section of test facility.

Tunnel stagnation temperatures are obtained by recording the output of four iridium-iridium (40 percent rhodium) thermocouples located at the downstream end of the combustion tube at various radial positions. The stagnation temperature is controlled by regulating the fuel-air ratio. Diametrical pitot-pressure surveys and stagnation-temperature surveys made over the length of the test region indicate a usable test core diameter of 2.5 to 3.0 inches (6.4 to 7.6 cm), dependent upon pressure. Over this diameter of the test core, there is a ±2-percent variation in pitot pressure and in total temperature (which corresponds to a maximum variation in Mach number of ±0.07).

For a given test run, the flow is started and allowed to reach the desired stagnation conditions. The model is then injected into the stream by means of a hydraulically actuated mechanism which requires approximately one-fourth second to position the model for testing. After data acquisition is completed, the model is removed from the test section.

The three hemisphere-cylinder models (models B, C, and D) and the delta wing-body model (model E) were tested over a range of stagnation conditions. Stagnation pressure was varied from about 700 to 1500 psia (4.83 to 10.3 MN/m^2) and the stagnation temperature varied from about 3300° to 3700° R (1833° to 2056° K). The variation of the resulting stream Reynolds number per foot (per 30.5 cm) was from about 0.4×10^6 to about 1.1×10^6. The nominal test Mach number was 7 with slight variation occurring with both pressure and temperature.

The hemisphere-cylinder models were tested primarily at an angle of attack of 0°. However, additional tests were made on the 0.395-inch-radius (1.003 cm) hemisphere (model B) for angles of attack from 0° to 19.6°. The delta wing-body model was tested for an angle-of-attack range of -19.5° to 20.1° at zero yaw angle and for an angle-of-attack range of -8.9° to 9.6° at a yaw angle of 10°. All models were injected into the established hypersonic flow with a predetermined attitude for a nominal test time interval of 6 seconds.

The linear variable differential transformer used to measure the volumetric expansion of the mercury in these tests (fig. 4(c)) indicated a linear output over a 0.44-inch (1.12-cm) stroke which is sufficient to measure the piston travel for the models tested. The instrumentation of the differential transformer consisted of a 3-kilocycle carrier-amplifier system which transferred variation of the output signal to variation in the d-c voltage. The variation in d-c voltage, as well as the tunnel reference data, was recorded by a galvanometer type of oscillograph recorder.

RESULTS AND DISCUSSION

Static Calibration

In order to establish the relation between net volumetric expansion and mean temperature rise of the liquid metal, each configuration to be considered must be statically calibrated.

Typical calibrations of various model configurations are plotted in figure 9. The solid curves in this figure represent percentages of the theoretical specific volumetric increase of the mercury, which would result from a given temperature rise if there were no expansion of the model shell. The relation between specific volume and temperature for mercury used for these calculations was that indicated by figure 3(a). The dashed curve in figure 9, which is located at a percentage level of 79 percent, represents the computed net expansion of the liquid metal when the model-shell expansion is considered for the flat-face cylinder model (model A). As can be seen from this figure, the experimental data agree well with the computed values for this configuration. The data from models B and C also fall close to this computed curve as a result of their volume and wall thickness being very close to that of model A. The reason that the volumetric expansion with temperature rise is lower for model D than for the other hemisphere-cylinder models is believed to be because of entrapped air. The model internal pressure increases with volume expansion because of the restraining force produced by the spring on the piston (fig. 4(c)) which was linear with distance displaced. The indicated net expansion of the mercury was reduced because of the compression of the entrapped air during the calibration. The further reduction of expansion with temperature rise for model E results from entrapped air and from greater shell expansion. The surface area per unit volume of liquid metal for this model was considerably greater than that for the hemisphere-cylinder models.

It should be pointed out that the task of filling these models completely with mercury without trapping air was extremely difficult because of the geometric shape of the shells and inner-wall roughness. In order to minimize the amount of air trapped, an attempt was made to fill the model within a high-vacuum environment. It was found that by use of the vacuum environment more consistent results were obtained.

Figure 9 shows that for the condition in which the shell and liquid metal are in thermal equilibrium, the effect of shell expansion and entrapped low-pressure air can be satisfactorily accounted for in the static calibration because of the linear relation between temperature rise and net expansion for all models considered. The fact that the data points plotted for model D were taken from two static calibration runs indicates good repeatability of the calibration technique.

Localized Heating Tests

The static calibration discussed in the preceding section adequately accounted for shell expansion and air bubbles inadvertently trapped in the shell volume provided the shell and liquid metal were in thermal equilibrium, which corresponds to a uniform shell expansion. For realistic cases of aerodynamic heating, where a large part of the total heat input to a body is highly localized, it was not clear that heat transfer rate between the shell and liquid metal would be fast enough to assume that the condition of thermal equilibrium was adequately maintained. Hence, a series of tests were performed where the total heat input to the model was highly localized, and the resulting heating rate indicated by volumetric expansion was compared with heating rates

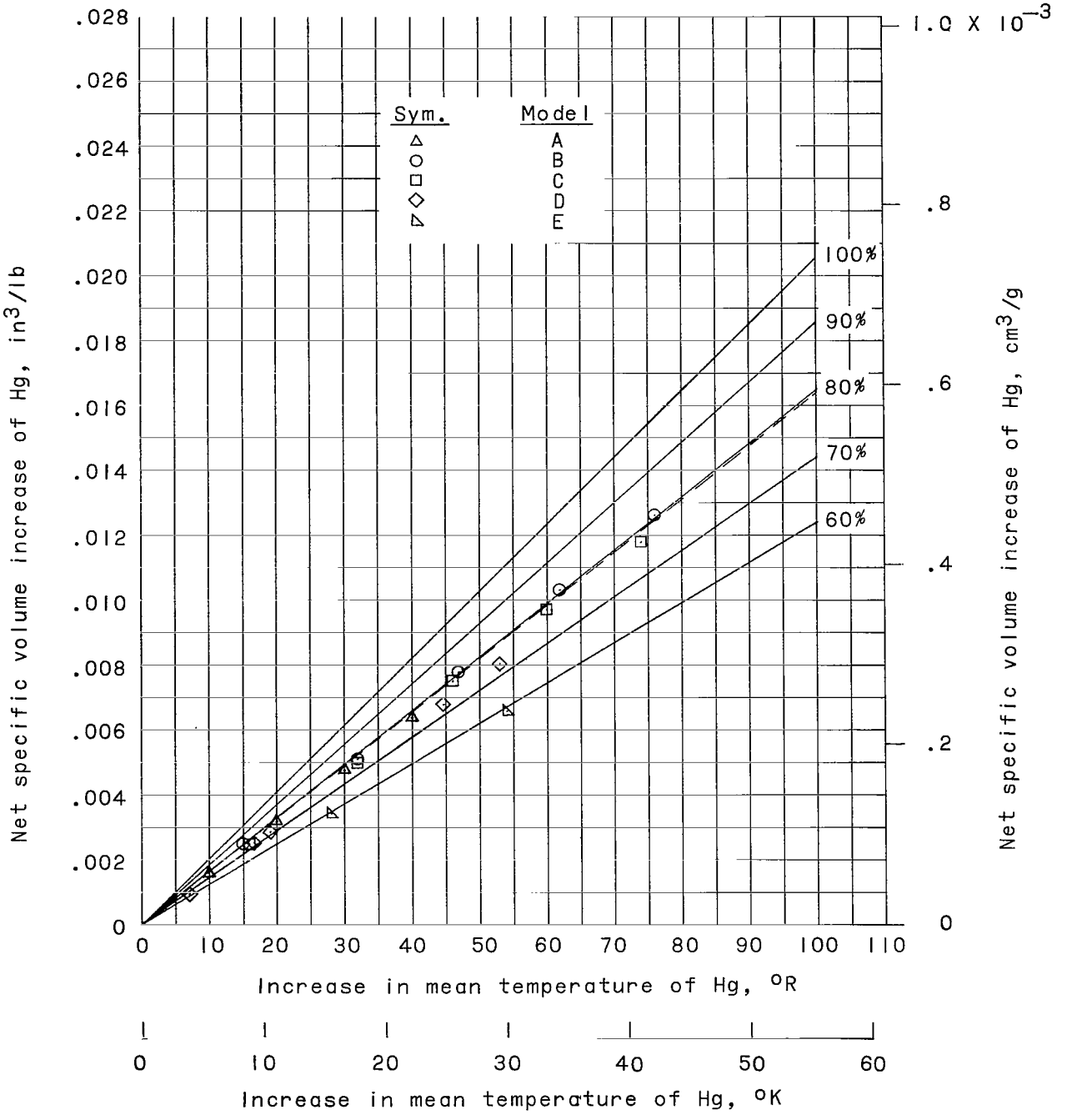

Figure 9.- Static calibration of net volumetric expansion of liquid mercury (Hg) with temperature increase for the different models.

determined by conventional means. In making this comparison, the value of $\frac{\partial V}{\partial \bar{T}}$ as defined by the static equilibrium calibration was used to reduce the data.

For the thermocouple instrumented plate which was used in the test with the quartz lamps, the local heating rate was obtained from the product of the density, specific heat, and wall thickness of the plate and the change in temperature per unit time as indicated by the thermocouple outputs; that is,

$$\dot{q} = \rho c_p \tau \frac{dT}{dt} \tag{2a}$$

For the arc-image furnace, the local heating rate was obtained from the product of the mass and specific heat of the copper calorimeter and the change in temperature of the calorimeter per unit time divided by the area of the model exposed to the radiant heating; that is,

$$\dot{q} = \frac{mc_p}{A_{ex}} \frac{dT}{dt} \tag{2b}$$

The data recorded for the liquid-metal expansion model during testing were in the form of pressure histories of the entrapped air located downstream of the piston (fig. 4(a)). The static calibration of the model gave a correlation between the liquid-metal (Hg) mean-temperature increase and the resultant piston travel. In this case, the volumetric expansion of the liquid metal was equal to the volumetric compression of the entrapped air. It should be noted that no experimental correlation was made between the volumetric compression and the resulting pressure increase of the entrapped air. This correlation was not made from the results of the static calibration of the model because of the error induced from the heating of the entrapped air by conduction from the oil bath. The compression of the entrapped air was assumed to occur isothermally; that is,

$$pV = \text{Constant} \tag{3}$$

This assumption is based on the fact that during these tests the cylinder surrounding the entrapped air was shielded from heating and remained cool. The excess heat, produced by the compression of the small volume of air, therefore, is believed to have been rapidly conducted into the effective heat sink provided by the cool container walls. Equation (3), which is a hyperbola, has a negative slope equal to the ratio of the volume to the pressure:

$$\frac{\partial V}{\partial p} = -\frac{V}{p}$$

However, for the pressure and volume used, the relationship between ∂p and ∂V was approximately linear. Therefore, the total heating rate recorded by the liquid-metal expansion model was reduced by using the following relation:

$$\dot{Q} = \int_S \dot{q}\, dS = mc_p \frac{\partial \overline{T}}{\partial V} \frac{\partial V}{\partial p} \frac{\partial p}{\partial t} \tag{4}$$

where $\frac{\partial \overline{T}}{\partial V}$ was experimentally determined (fig. 9), $\frac{\partial V}{\partial p}$ was the linear isothermal relation of incremental volume and pressure of the air assumed, and $\frac{\partial p}{\partial t}$ was determined from the history of the pressure transducer output.

Pertinent data from the radiant heating test are presented in table I. The heating rate $\dot{q}$ presented is that determined from the thermocouple

TABLE I

PERTINENT DATA FROM RADIANT TESTS OF THE FLAT-FACE CYLINDER MODEL

Radiation test	$\dot{q}$		$\dot{Q}$	
	Btu/ft^2-sec	MW/m^2	Btu/sec	W
Quartz-lamp facility; A_{ex} = 0.0058 ft^2 (5.38 cm^2)				
1	79.0	0.897	0.471	497
2	52.1	.591	.251	265
3	68.5	.777	.345	364
4	61.2	.695	.340	359
5	55.4	.629	.321	339
6	24.5	.278	.121	127
7	32.3	.367	.171	180
8	48.1	.546	.256	270
9	53.0	.601	.267	282
10	67.0	.760	.390	411
11	77.0	.874	.432	456
12	13.8	.157	.0768	81.0
13	18.5	.210	.0861	90.8
14	19.8	.225	.118	124
15	13.2	.150	.0609	64.3
Small arc-image furnace; A_{ex} = 0.000341 ft^2 (0.317 cm^2)				
16	199.5	2.264	------	----
17	173.5	1.969	------	----
18	183.0	2.077	------	----
19	-----	-----	0.0697	73.5
20	-----	-----	.0675	71.2

instrumented plate or the copper button calorimeter, depending on the facility used. The total heating rate $\dot{Q}$ presented is the quantity determined from the liquid-metal expansion technique. The ratio of the total heating rate to the exposed area of the flat-face model is the indicated heating rate per unit area afforded by the present technique. The data obtained in each of the heating facilities are plotted in figure 10. The ratio of the total heating rate

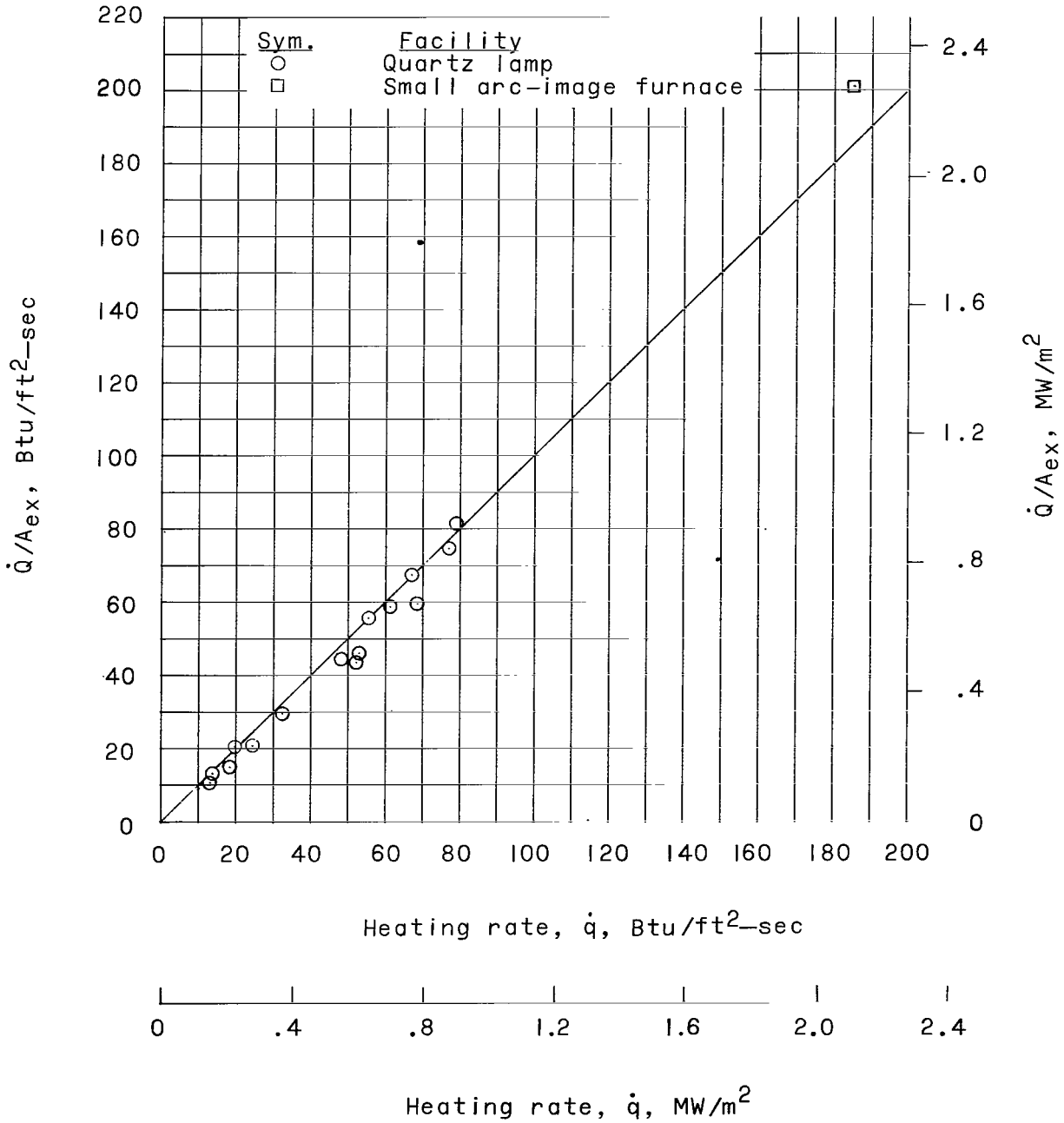

Figure 10.- Comparison of heating rate as afforded by liquid-metal expansion technique with that indicated by reference techniques.

recorded to the exposed area is plotted against the local heating rate determined by conventional reference methods. The heating rate obtained with the liquid-metal expansion technique agrees with that indicated by the reference techniques to within about ±10 percent. It is also indicated that the mean temperature of the model shell remains fairly close to the mean temperature of the contained liquid metal, as is evidenced by the fact that the static calibration data for thermal equilibrium conditions used to reduce the heating data produced heating rates in good agreement with those afforded by the reference techniques. These results lend confidence to the use of the static calibration in the reduction of aerodynamic heating data.

Aerodynamic Heating Test

The total aerodynamic heating rates to the three hemisphere-cylinder models (models B, C, and D) and the delta wing-body model (model E) were measured. For each model test, the recorded output of the linear variable differential transformer was used to obtain the history of the piston travel. Two typical histories are shown as figure 11. The relation between the increase in mean temperature of the liquid metal (Hg) and the piston travel, indicated by the dual scales in the figure, was established from the static calibration of the models (fig. 9).

The slope of volume variation with time $\left(\frac{\partial V}{\partial t}\right)$, needed to make the total-heating-rate determination (eq. (1)), and the tunnel reference measurements were evaluated for each run during a time interval between 3 and 6 seconds. (See fig. 11.) For about the inital 3 seconds, the recorded piston travel was affected by the inconsistent friction on the piston and spring and the initial lag in the system. After about a 3-second elapse of run time, $\frac{\partial V}{\partial t}$ was effectively constant for a time interval of 2 to 3 seconds. The fact that $\frac{\partial V}{\partial t}$ is constant for a given interval indicates that during that time the total heating rate was also approximately constant since the mercury acts as a heat sink and keeps the wall-temperature increase relatively small. Inasmuch as the average stagnation-point wall temperature for the 2-second interval generally increased approximately 50° R (27.8° K), the total heating rate would decrease less than 2 percent for this interval.

In order to account for small variations in tunnel stagnation conditions, the model stagnation-point heating rate computed for tunnel conditions was used as the reference in presenting the data. This stagnation-point heating rate was derived by the method of Fay and Riddell (ref. 5) by taking into account the actual transport and flow properties of the combustion products (ref. 6). The theoretical values so computed are in agreement with experimental data, as obtained from measurements at the stagnation point of "thin wall" hemispheres tested in the 7-inch Mach 7 pilot tunnel. The theoretical predictions are compared directly with experimental results in figure 12. It is indicated by this figure that the stagnation-point heating rate for hemispheres as tested in this facility can be predicted by theory to within ±10 percent.

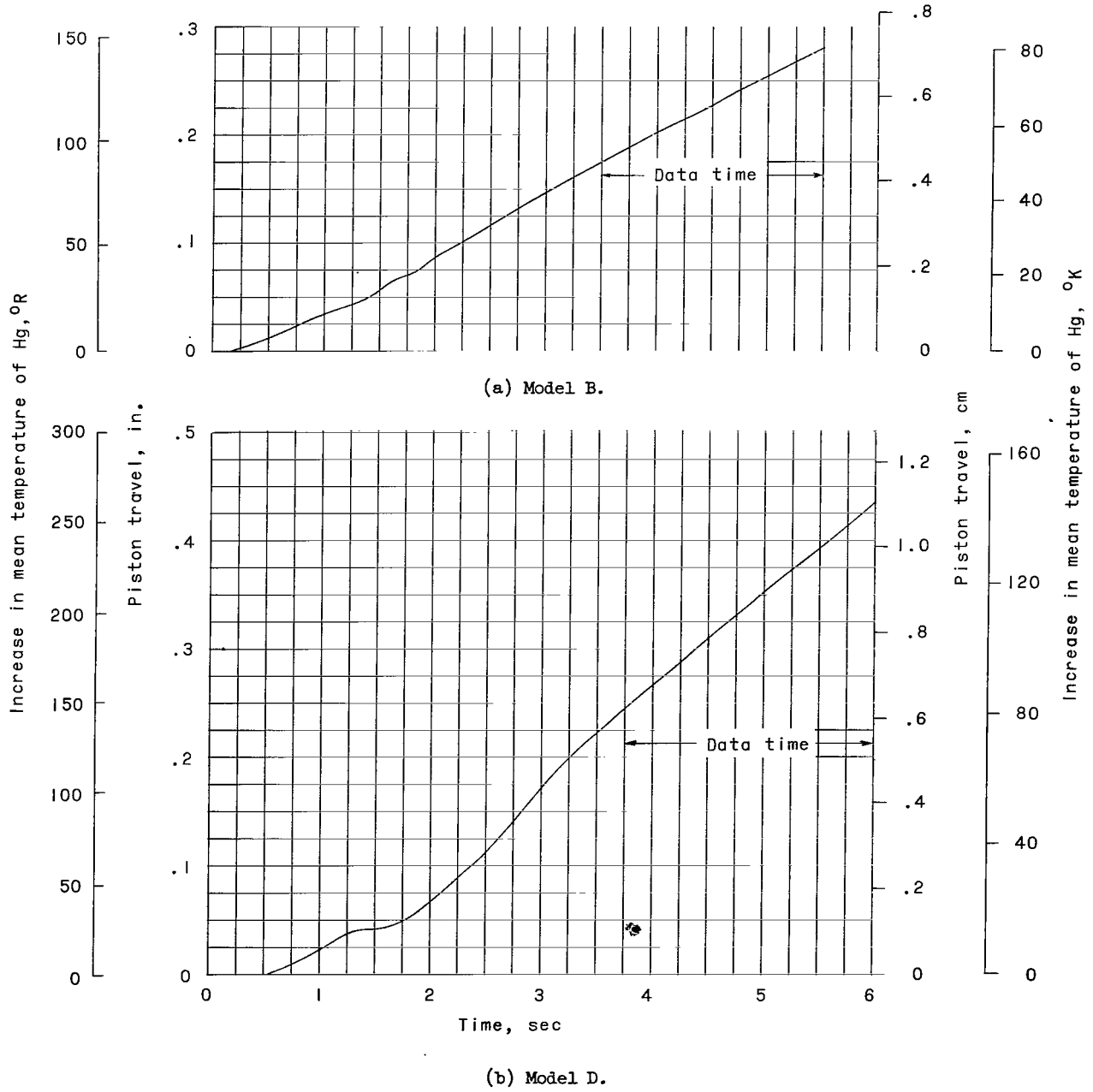

(a) Model B.

(b) Model D.

Figure 11.- Typical output data histories from two hemisphere-cylinder models containing equal volumes of mercury as obtained from aerodynamic heating tests.

In order to evaluate $\dot{q}_s$ for the hemisphere-cylinder models, the inside wall temperature at the stagnation point was measured for three test runs (aerodynamic tests 15, 16, and 17 of table II) for mercury-filled model C by using a chromel-alumel thermocouple attached to the inner surface of the wall at the stagnation point. The measured wall temperatures were correlated with the tunnel stagnation conditions and test time elapsed. From this correlation, approximate stagnation-point wall temperatures were obtained with which values of $\dot{q}_s$ could be computed.

The $\dot{q}_s$ of the delta wing-body model was evaluated by using a stagnation-point wall temperature of 1460° R (811° K). This temperature was approximated from a knowledge of the surface temperatures occurring during the test made with the hemisphere-cylinder models.

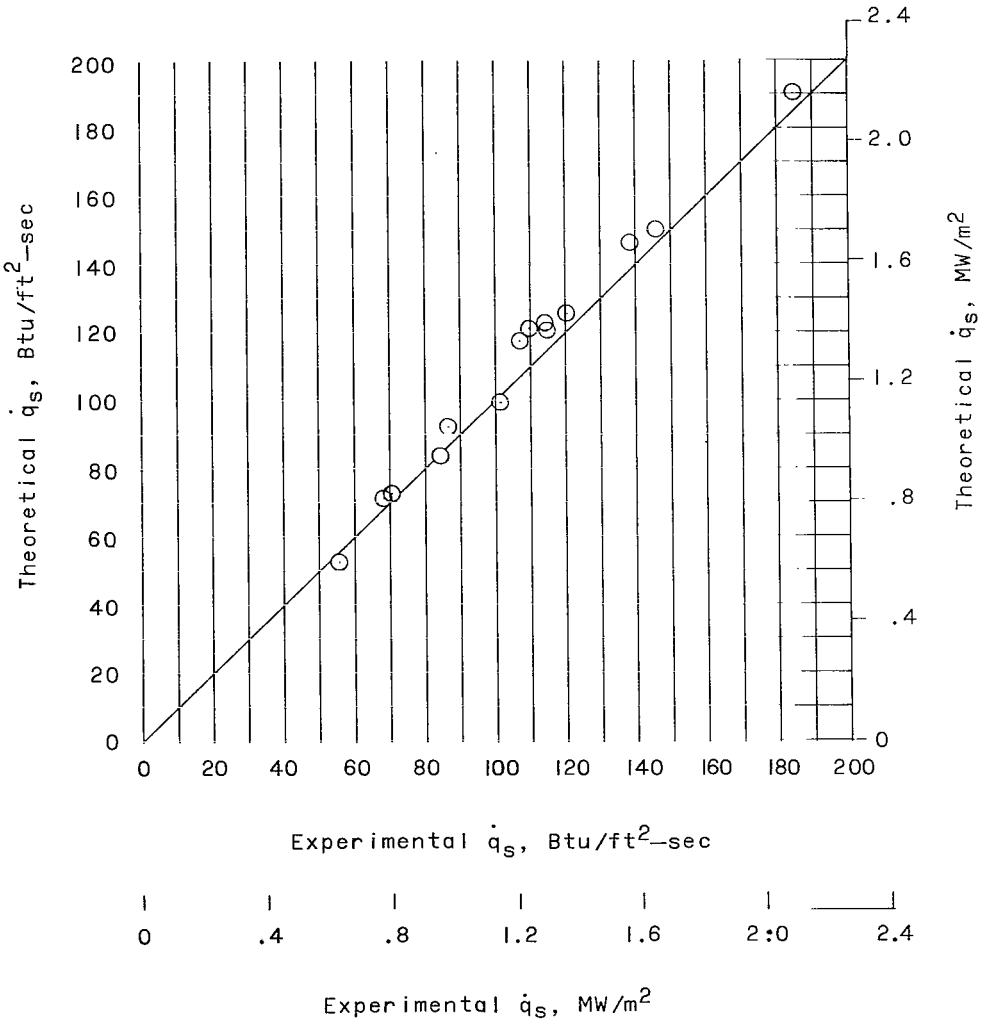

Figure 12.- Comparison of theoretical stagnation-point heating rate on a hemisphere with that measured experimentally.

Pertinent data from the aerodynamic heating tests are presented in tables II and III. In table II all data from tests on the hemisphere-cylinder models, including model geometric dimensions, model attitude during test, and tunnel stagnation conditions, are listed. The stagnation-point wall temperature T_{ws}, used to compute $\dot{q}_s$, was deduced as previously described. Table III presents the data from tests of the delta wing-body model. In this table, the model attitude (described by the angle-of-attack and yaw settings), the tunnel reference conditions, and the stagnation-point heating rate $\dot{q}_s$ are listed.

TABLE II

PERTINENT DATA FROM AERODYNAMIC TESTS OF THE HEMISPHERE-CYLINDER MODELS

Aerodynamic test	α, deg	p_t		T_t		T_{ws}		$\dot{q}_s$		$\dot{Q}$	
		psia	MN/m^2	^oR	^oK	^oR	^oK	Btu/ft^2-sec	MW/m^2	Btu/sec	W
r = 0.395 in. (1.003 cm); $\frac{l}{r}$ = 6.07											
1	0	1005	6.93	3570	1983	1330	739	123.1	1.40	0.519	548
2	0	993	6.85	3570	1983	1330	739	122.9	1.39	.514	542
3	0	1001	6.90	3505	1947	1320	733	119.0	1.35	.499	526
4	0	1001	6.90	3420	1900	1310	728	113.2	1.28	.480	506
5	0	979	6.75	3470	1926	1320	733	122.0	1.38	.512	540
6	5	1001	6.90	3445	1914	1320	733	115.0	1.31	.496	523
7	10	1001	6.90	3535	1964	1330	739	121.0	1.37	.517	545
8	10	1005	6.93	3505	1947	1320	733	117.5	1.33	.512	540
9	10	979	6.75	3505	1947	1330	739	117.4	1.33	.556	587
10	19.6	971	6.69	3455	1919	1320	733	118.3	1.34	.645	680
11	19.6	970	6.69	3495	1941	1320	733	119.8	1.36	.655	691
r = 0.645 in. (1.637 cm); $\frac{l}{r}$ = 0.93											
12	0	1018	7.02	3530	1961	1260	700	98.3	1.12	0.789	832
13	0	1005	6.93	3470	1928	1250	694	96.0	1.09	.763	805
14	0	1005	6.93	3390	1883	1230	683	91.3	1.04	.723	763
15	0	968	6.67	3480	1933	1240	689	93.3	1.06	.742	783
16	0	975	6.72	3330	1850	1210	672	86.2	.98	.697	735
17	0	1468	10.12	3720	2066	1200	667	125.0	1.42	1.014	1070
r = 0.770 in. (1.953 cm); $\frac{l}{r}$ = 0.29											
18	0	984	6.78	3500	1944	1180	656	90.6	1.03	0.967	1020
19	0	984	6.78	3540	1966	1190	661	91.3	1.04	1.002	1057
20	0	705	4.86	3410	1894	1100	611	75.4	.86	.740	781
21	0	979	6.75	3520	1955	1210	672	89.6	1.02	.922	973
22	0	674	4.65	3580	1989	1140	633	80.2	.91	.756	798
23	0	958	6.61	3520	1955	1210	672	88.9	1.01	.927	978
24	0	687	4.74	3560	1978	1160	644	79.5	.90	.885	934
25	0	803	5.54	3550	1972	1180	656	84.2	.96	.870	918

TABLE III

PERTINENT DATA FROM AERODYNAMIC TESTS OF THE DELTA WING MODEL

Aerodynamic test	α, deg	ψ, deg	p_t		T_t		$\dot{q}_s$		$\dot{Q}$	
			psia	MN/m^2	$^\circ$R	$^\circ$K	Btu/ft^2-sec	MW/m^2	Btu/sec	W
27	1.0	0	953	6.57	3635	1764	212	2.41	0.860	907
28	1.0	0	953	6.57	3670	1783	223	2.53	.806	850
29	1.0	0	937	6.46	3460	1667	190	2.16	.735	775
30	1.0	0	986	6.80	3530	1705	159	1.80	.644	679
31	1.0	0	983	6.78	3510	1694	158	1.79	.680	717
32	1.0	0	1371	9.45	3725	1814	264	3.00	.985	1039
33	1.0	0	1384	9.54	3710	1805	263	2.98	.995	1050
34	-9.8	0	989	6.82	3410	1639	189	2.14	.880	928
35	-9.8	0	989	6.82	3480	1678	198	2.25	.897	946
36	-19.5	0	989	6.82	3410	1639	189	2.14	1.003	1058
37	-19.5	0	971	6.70	3410	1639	187	2.12	1.038	1095
38	10.4	0	976	6.73	3350	1605	179	2.03	.728	768
39	10.4	0	961	6.63	3445	1658	189	2.14	.763	805
40	20.1	0	971	6.70	3420	1644	187	2.12	.828	874
41	20.1	0	971	6.70	3410	1639	187	2.12	.828	874
42	0	10	976	6.73	3430	1650	190	2.16	.816	861
43	0	10	976	6.73	3460	1667	193	2.19	.816	861
44	-8.9	10	976	6.73	3470	1672	194	2.20	.902	952
45	-8.9	10	976	6.73	3450	1661	192	2.18	.929	980
46	9.6	10	971	6.70	3510	1694	200	2.27	.869	917
47	9.6	10	971	6.70	3500	1689	199	2.26	.869	917

Hemisphere-cylinder models.- The three hemisphere-cylinder models form a family of bodies having a fixed volume as defined by their external shape. Any variation in total heating rate between the models, then, is caused by the change in length-diameter ratio only, inasmuch as the volume and basic geometry are fixed.

An analytical expression for the total heating rate to a hemisphere-cylinder model immersed in hypersonic flow is

$$\dot{Q} = \int_S \dot{q}\, dS = 2\pi r^2 \dot{q}_s \int_0^{\frac{s}{r}} \frac{\dot{q}}{\dot{q}_s} \sin\theta \, d\left(\frac{s}{r}\right)$$

or, nondimensionalized,

$$\frac{\dot{Q}}{\dot{q}_s r^2} = 2\pi \int_0^{\frac{s}{r}} \frac{\dot{q}}{\dot{q}_s} \sin\theta \, d\left(\frac{s}{r}\right) \tag{5}$$

For a fixed hemisphere-cylinder geometry, the total heating rate parameter $\frac{\dot{Q}}{\dot{q}_s r^2}$ is a function only of the heating distribution of $\dot{q}/\dot{q}_s$. For Newtonian analysis at hypersonic speeds, the distribution of $\dot{q}/\dot{q}_s$ on such bodies varies only slightly with Mach number. The Mach number effect appears as a change in level of heating at and downstream of the hemisphere-cylinder shoulder. Inasmuch as the present tests were performed at a fixed Mach number, the total heating rate parameter should be a constant for each hemisphere-cylinder model.

Figure 13 presents the total heating rate parameter for the three hemisphere-cylinder models at zero angle of attack plotted against the stagnation-point heating rate, where the values of $\dot{q}_s$ were derived by means of the procedures discussed earlier in this section of the paper. The total heating rate parameters which were obtained by integrating the experimentally determined heating rate distribution from a "thin skin" hemisphere-cylinder heat-transfer model (ref. 7) are presented for the geometries of models C and D as the dashed lines. Theoretical total heating rate parameters computed according to reference 8 are presented as the solid lines.

The data in figure 13 indicate that the total heating rate parameter $\frac{\dot{Q}}{\dot{q}_s r^2}$ is indeed a constant for a fixed hemisphere-cylinder model. More important is the indication that the present technique provides total-heating-rate data in good agreement with those obtained from current methods of defining total heating rate and with theory. The differences between the various data values are well within the accuracy of the theory and the two experimental techniques. The scatter in data from model D is believed to be caused by the previously discussed entrapped air in the model shell volume, which resulted in an effective degree of compressibility for the liquid metal. This "sponginess" resulted in erratic movement of the piston and some scatter in repeatability.

The effect of length-radius ratio l/r on the total heating rate parameter is shown in figure 14. Here again the experimental results from the present technique are compared with the total heating rate determined from integration of the experimental heating rate distributions and with theory. Note that the total heating rate parameter increases significantly as l/r increases (in effect, as the volume is stretched out into a cylinder). It should be pointed out that although the value of $\frac{\dot{Q}}{\dot{q}_s r^2}$ increases, the total heating rate $\dot{Q}$ decreases. For the constant volume case, as l/r is increased r must decrease directly. The present data are replotted in the dimensional form $\dot{Q}/\dot{q}_s$ and presented in figure 15 to provide a clearer indication of the variation of the total heating rate with l/r for the hemisphere-cylinder model.

As stated previously, model B, in addition to being tested at zero angle of attack, was also tested at angles of attack up to 19.6°. The tests were

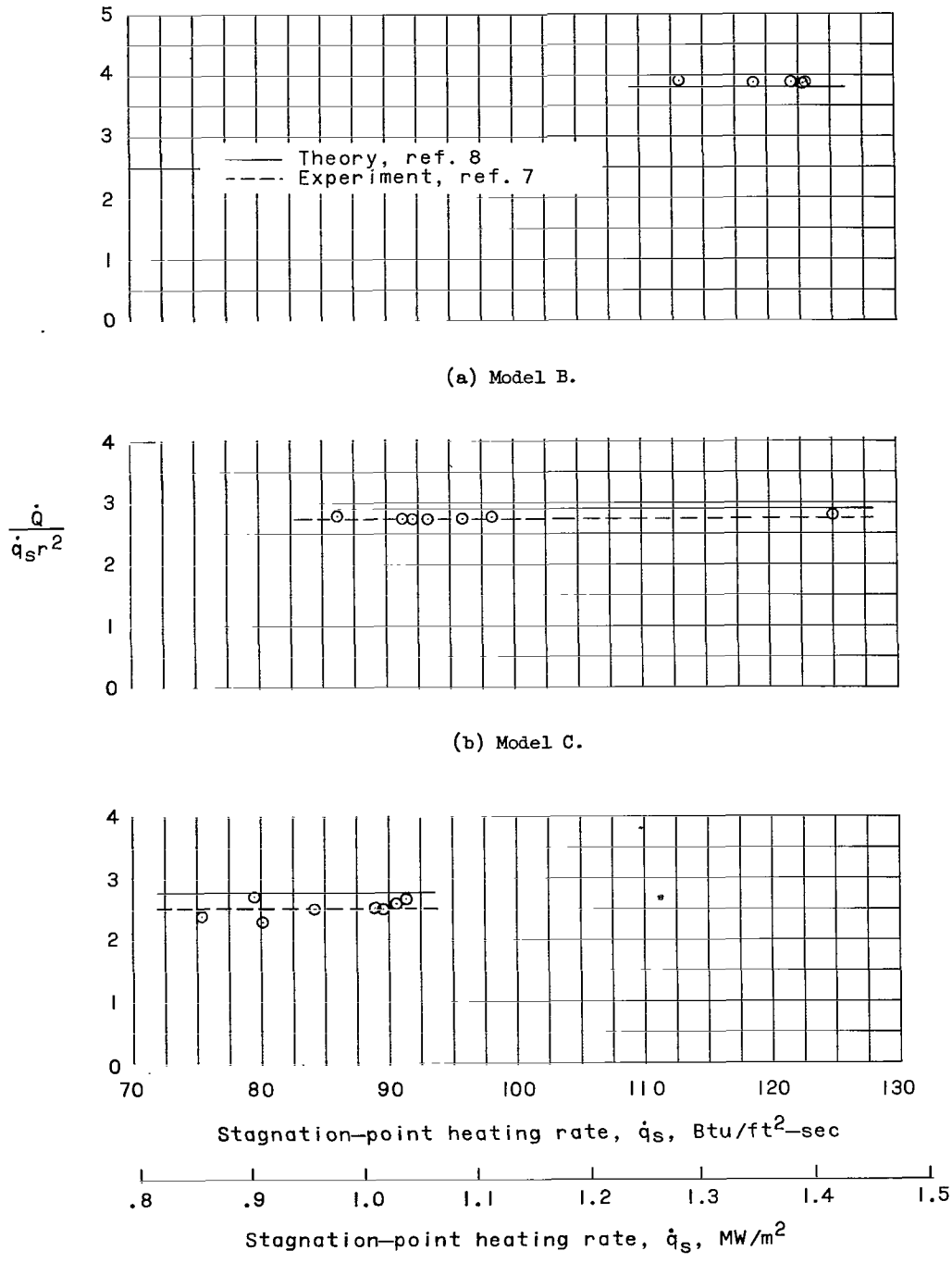

(a) Model B.

(b) Model C.

(c) Model D.

Figure 13.- Variation of total heating rate parameter with stagnation-point heating rate for three hemisphere-cylinder models. $\alpha = 0^{\circ}$.

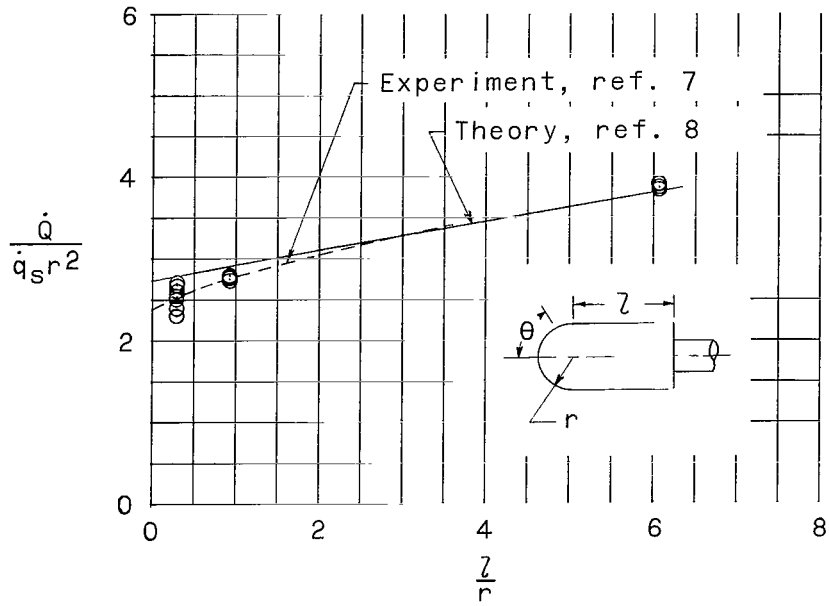

Figure 14.- Variation of total heating rate parameter with length-radius ratio of hemisphere-cylinder model for a constant volume. $\alpha = 0^{\circ}$.

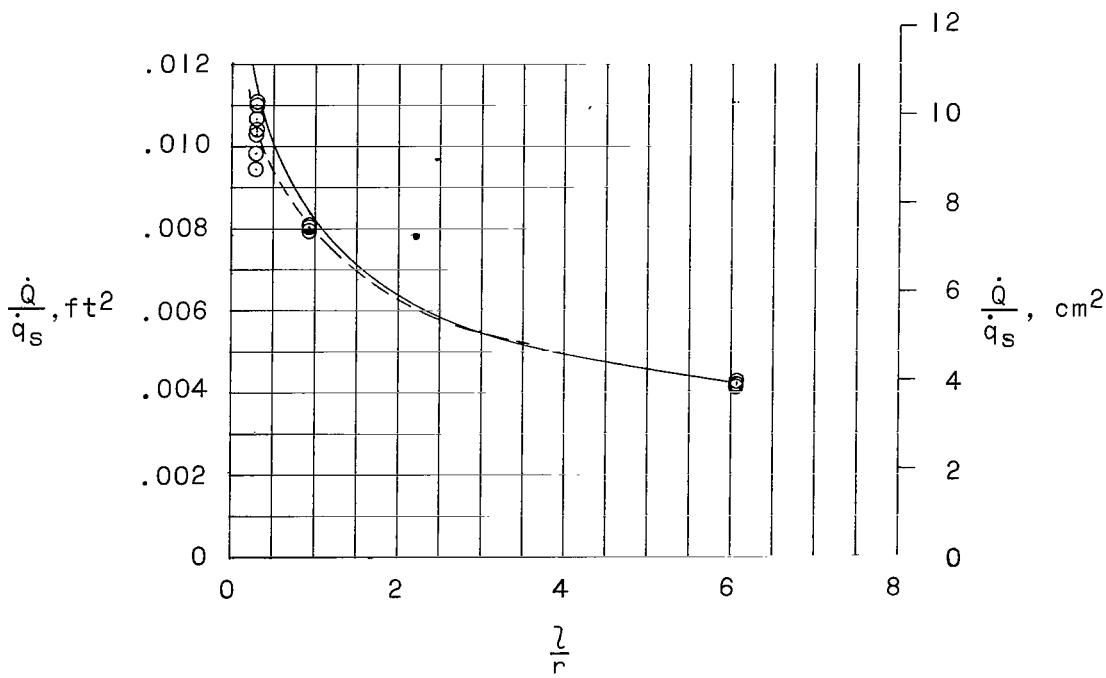

Figure 15.- Variation of ratio of total heating rate to stagnation-point heating rate with length-radius ratio of hemisphere-cylinder model for a constant volume. $\alpha = 0^{\circ}$.

made to indicate the change in total heating rate resulting from imposing angle-of-attack conditions on simple bodies. The results of these tests are presented in figure 16 where the total heating rate parameter is plotted against angle of attack. It appears from the data shown for this body that small angles of attack can be tolerated without significant change in total heating rate. However, at an angle of attack near 20° the heating rate parameter was indicated to be 25 percent greater than that at an angle of attack of 0°.

Delta wing-body model.- The delta wing-body model was tested to determine whether a consistent set of experimental total-heating-rate data for such configurations could be obtained from the present measuring technique. The absolute level of the total heating rate for this configuration could not be derived theoretically, and experimental heating rate distributions are not available from which to obtain an experimental value. Hence, the experimental results are presented without comparative data.

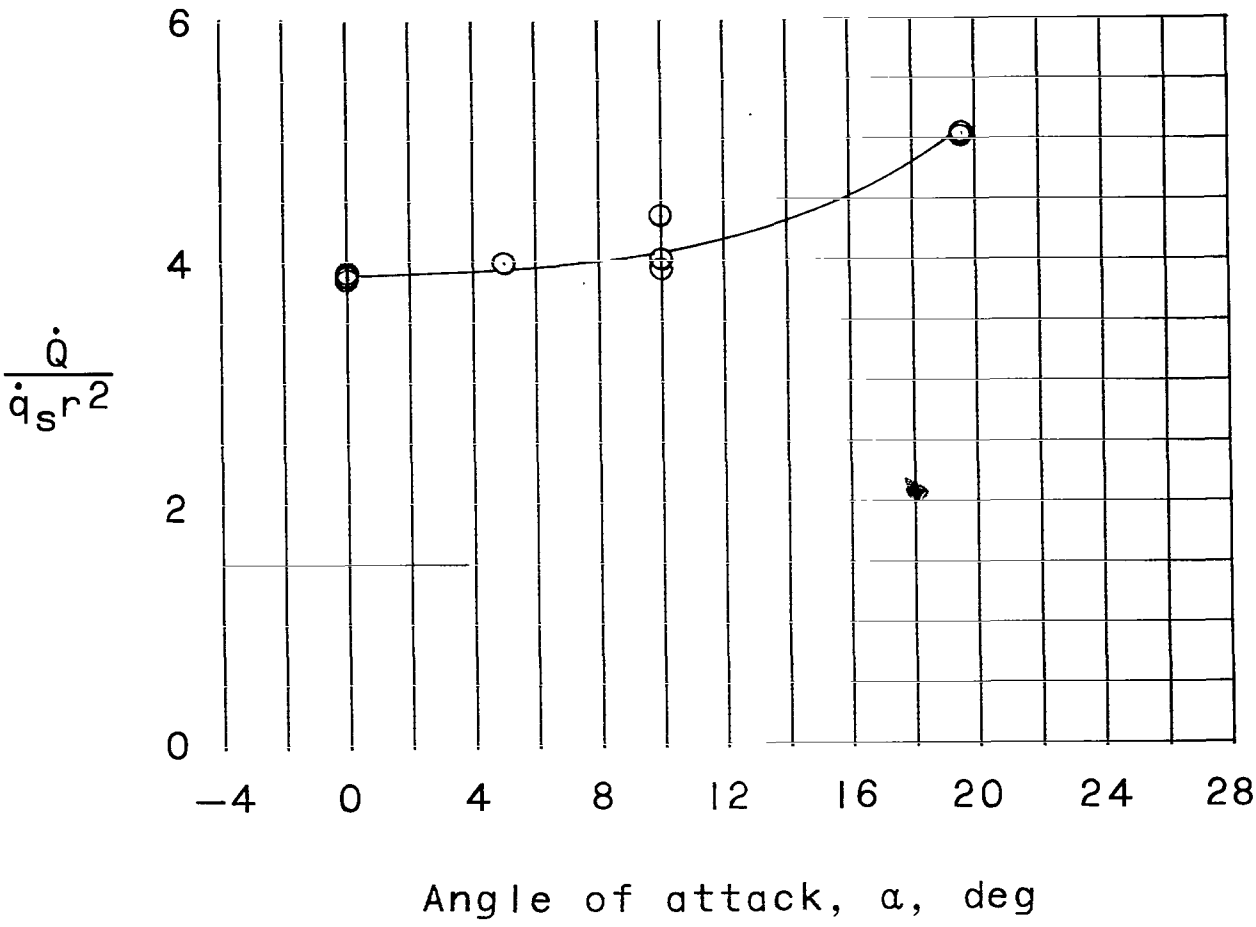

Figure 16.- Variation of total heating rate parameter with angle of attack for model B.

The total heating rate parameter for the delta wing-body model E, at an angle of attack of 1° (nominal value of zero) and zero yaw, is plotted against its stagnation-point heating rate in figure 17. For a fixed hypersonic Mach number, the total heating rate for such complex configurations is a function only of body stagnation-point conditions, as was also indicated to be the case for the simple hemisphere-cylinder bodies. Figure 18 presents the variation of total-heating-rate data with angles of attack for model E at fixed angles of yaw of 0° and 10°. The data show that this particular configuration has a minimum value of the total heating rate parameter near zero angle of attack and that the rate parameter increases with both positive and negative angles of attack. The greater rate of total-heating-rate-parameter increase with negative angle of attack is believed to reflect principally the greater wetted area on the upper surface of the body. The fixed angle of yaw of 10° apparently increased the value of the total heating rate parameter a fixed amount throughout the angle-of-attack range presented. Generally, the data presented in figures 17 and 18 show trends in heating rate that were about as would be expected. The repeatability of the data was very good as indicated by the data points in these plots.

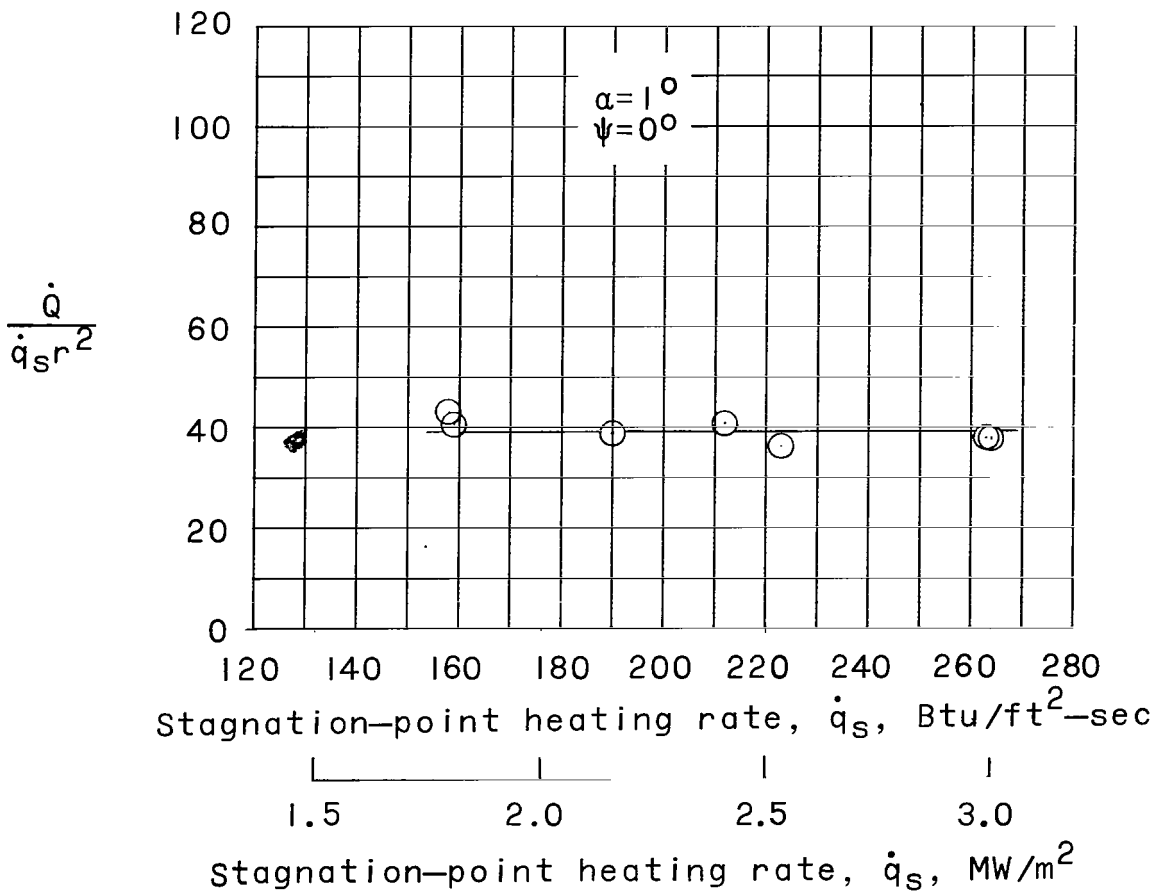

Figure 17.- Variation of total heating rate parameter with stagnation-point heating rate for model E.

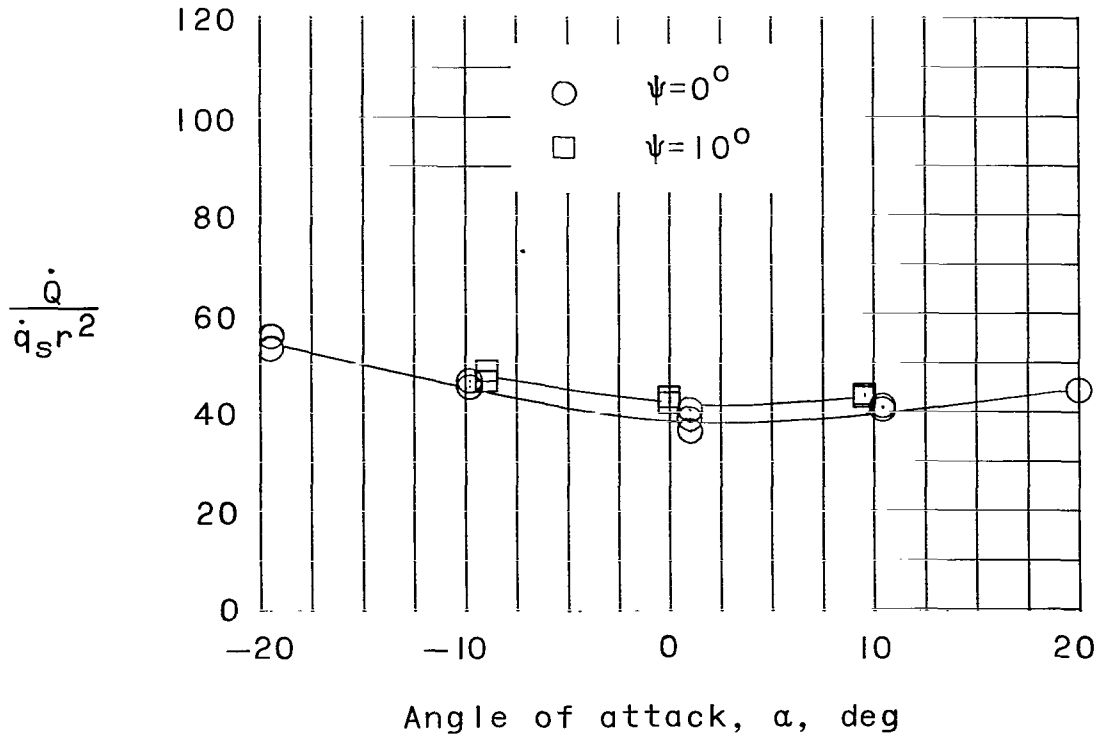

Figure 18.- Variation of total heating rate parameter with angle of attack for model E.

The results from these aerodynamic tests are belived to indicate that the technique as described and demonstrated herein will accurately indicate the total heating rates to bodies of arbitrary shape and attitude. Use of the technique should permit experimental studies of total heating rates to complex bodies to be made more rapidly and more accurately than has been possible heretofore.

CONCLUDING REMARKS

A liquid-metal expansion technique for measuring the total aerodynamic heating rate to bodies of arbitrary shape has been described. The calibration and test procedures required to gain useful knowledge from the technique have been delineated. In addition, the results obtained from three types of apparatus have been presented to demonstrate the accuracy and reliability of the technique.

Because of the "integrating" performed by the liquid metal, total heating rate is determined by one measurement. The resulting simplicity of model and instrumentation enhance the technique as a means of easily obtaining reliable total-heating-rate data. Use of the technique should accurately measure the total aerodynamic heating rates to simple configurations such as hemisphere-cylinder models as well as afford measurements of the total heating rate to three-dimensional bodies for a wide range of possible heating rate distributions.

The technique is sufficiently sensitive to indicate the effect of angle of attack or yaw on the total heating rates to both simple hemisphere-cylinder models and more complex delta wing-body models.

Langley Research Center,
National Aeronautics and Space Administration,
Langley Station, Hampton, Va., May 18, 1964.

APPENDIX A

CONVERSION OF U.S. CUSTOMARY UNITS TO SI UNITS

The International System of Units, abbreviated SI (Systeme International), was adopted in 1960 by the Eleventh General Conference on Weights and Measures held in Paris, France. (See ref. 2) Conversion factors required for units used herein are given in the following table:

Physical quantity	U.S. customary unit	Conversion factor (*)	SI unit
Absolute viscosity	lb/ft-sec	1.488	newton-seconds/meter^2 (Ns/m^2)
Area	ft^2	9.29×10^{-2}	meters^2 (m^2)
Length	in.	0.0254	meters (m)
	ft	0.3048	meters (m)
Local heating rate	Btu/ft^2-sec	1.135×10^4	watts/meter^2 (W/m^2)
Pressure	psia	6.895×10^3	newtons/meter^2 (N/m^2)
Specific heat	Btu/lb-$^\circ$R	4.184	joules/gram-degrees Kelvin (J/g-$^\circ$K)
Specific volume	in.^{3}/lb	3.613×10^{-8}	meters^3/gram (m^3/g)
Surface tension	lb/ft	14.59	newtons/meter (N/m)
Temperature	$^\circ$R	5/9	degrees Kelvin ($^\circ$K)
	($^\circ$F + 459.67)	5/9	degrees Kelvin ($^\circ$K)
Thermal conductivity	Btu/sec-ft-$^\circ$R	43.24	watts/meter-degrees Kelvin (W/m-$^\circ$K)
Total heating rate	Btu/sec	1.055×10^3	watts (W)

*Multiply value given in U.S. customary unit by conversion factor to obtain equivalent value in SI unit.

Prefixes to indicate multiples of units are as follows:

Prefix	Multiple
mega (M)	10^6
kilo (k)	10^3
centi (c)	10^{-2}
milli (m)	10^{-3}
micro (μ)	10^{-6}

REFERENCES

1. Chapman, Gary T., and Jackson, Charles T., Jr.: Measurement of the Heat Transfer to Bodies of Revolution in Free Flight by Use of a Catcher Calorimeter. NASA TN D-1890, 1963.

2. Anon.: International System of Units, Resolution No. 12. NASA TT F-200, 1964.

3. Lyon, Richard N., ed.: Liquid-Metals Handbook. Second ed., NAVEXOS P-733 (rev.), Atomic Energy Comm. and Dept. Navy, June 1952.

4. Jackson, Carey B., ed.: Liquid Metals Handbook - Sodium (NaK) Supplement. Atomic Energy Comm. and Dept. Navy, July 1955, p. 32.

5. Fay, J. A., and Riddell, F. R.: Theory of Stagnation Point Heat Transfer in Dissociated Air. Jour. Aero. Sci., vol. 25, no. 2, Feb. 1958, pp. 73-85, 121.

6. Leyhe, E. W., and Howell, R. R.: Calculation Procedure for Thermodynamic, Transport, and Flow Properties of the Combustion Products of a Hydrocarbon Fuel Mixture Burned in Air With Results for Ethylene-Air and Methane-Air Mixtures. NASA TN D-914, 1962.

7. Weinstein, Irving: Heat Transfer and Pressure Distributions on a Hemisphere-Cylinder and a Bluff-Afterbody Model in Methane-Air Combustion Products and in Air. NASA TN D-1503, 1962.

8. Kemp, Nelson H., Rose, Peter H., and Detra, Ralph W.: Laminar Heat Transfer Around Blunt Bodies in Dissociated Air. Jour. Aero/Space Sci., vol. 26, no. 7, July 1959, pp. 421-430.

NASA-Langley, 1964 L-3953

"The aeronautical and space activities of the United States shall be conducted so as to contribute . . . to the expansion of human knowledge of phenomena in the atmosphere and space. The Administration shall provide for the widest practicable and appropriate dissemination of information concerning its activities and the results thereof."

—NATIONAL AERONAUTICS AND SPACE ACT OF 1958

NASA SCIENTIFIC AND TECHNICAL PUBLICATIONS

TECHNICAL REPORTS: Scientific and technical information considered important, complete, and a lasting contribution to existing knowledge.

TECHNICAL NOTES: Information less broad in scope but nevertheless of importance as a contribution to existing knowledge.

TECHNICAL MEMORANDUMS: Information receiving limited distribution because of preliminary data, security classification, or other reasons.

CONTRACTOR REPORTS: Technical information generated in connection with a NASA contract or grant and released under NASA auspices.

TECHNICAL TRANSLATIONS: Information published in a foreign language considered to merit NASA distribution in English.

TECHNICAL REPRINTS: Information derived from NASA activities and initially published in the form of journal articles.

SPECIAL PUBLICATIONS: Information derived from or of value to NASA activities but not necessarily reporting the results of individual NASA-programmed scientific efforts. Publications include conference proceedings, monographs, data compilations, handbooks, sourcebooks, and special bibliographies.

Details on the availability of these publications may be obtained from:

SCIENTIFIC AND TECHNICAL INFORMATION DIVISION

NATIONAL AERONAUTICS AND SPACE ADMINISTRATION

Washington, D.C. 20546